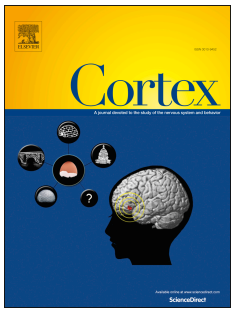

Functional dysregulation of the auditory cortex in bilateral perisylvian polymicrogyria: multiparametric case analysis of the absent speech phenotype

Dominika Slušná, Jiwandeep Singh Kohli, Janice Hau, Juan Álvarez-Linera Prado, Annika Carola Linke, Wolfram Hinzen

PII: S0010-9452(23)00292-7

DOI: https://doi.org/10.1016/j.cortex.2023.11.006

Reference: CORTEX 3814

To appear in: *Cortex*

Received Date: 20 June 2023

Revised Date: 23 October 2023

Accepted Date: 2 November 2023

Please cite this article as: Slušná D, Kohli JS, Hau J, Álvarez-Linera Prado J, Linke AC, Hinzen W, Functional dysregulation of the auditory cortex in bilateral perisylvian polymicrogyria: multiparametric case analysis of the absent speech phenotype, *CORTEX*, https://doi.org/10.1016/j.cortex.2023.11.006.

Functional dysregulation of the auditory cortex in bilateral perisylvian polymicrogyria: multiparametric case analysis of the absent speech phenotype

Dominika Slušná [a, *], Jiwandeep Singh Kohli [b], Janice Hau [b], Juan Álvarez-Linera Prado [c], Annika Carola Linke [b], Wolfram Hinzen [a, d]

[a] *Department of Translation and Language Sciences, Campus Poblenou, Pompeu Fabra University, Barcelona, Spain*

[b] *Brain Development Imaging Laboratories, Department of Psychology, San Diego State University, San Diego, CA, USA*

[c] *Neuroradiology Department, Hospital Ruber Internacional, Madrid, Spain*

[d] *Institució Catalana de Recerca I Estudis Avancats, ICREA, Barcelona, Spain*

* Corresponding author at Department of Translation and Language Sciences, Campus Poblenou, Pompeu Fabra University, office #53.712, 08018, Barcelona, Spain. E-mail address: slusnadominika@gmail.com. Orcid ID: **0000-0002-4886-7397**

Abstract

The absence of speech is a clinical phenotype seen across neurodevelopmental syndromes, offering insights for neural language models. We present a case of bilateral perisylvian polymicrogyria (BPP) and complete absence of speech with considerable language comprehension and production difficulties. We extensively characterized the auditory speech perception and production circuitry by employing a multimodal neuroimaging approach. Results showed extensive cortical thickening in motor and auditory-language regions. The auditory cortex lacked sensitivity to speech stimuli despite relatively preserved thalamic projections yet had no intrinsic functional organization. Subcortical structures implicated in early stages of processing exhibited heightened sensitivity to speech. The arcuate fasciculus, a suggested marker of language in BPP, showed similar volume and integrity to a healthy control. The frontal aslant tract, linked to oromotor function, was partially reconstructed. These findings highlight the importance of assessing the auditory cortex beyond speech production structures to understand absent speech in BPP. Despite profound cortical alterations, the intrinsic motor network and motor-speech pathways remained largely intact. This case underscores the need for comprehensive phenotyping using multiple MRI modalities to uncover causes of severe disruption in language development.

Keywords: cortical development, fMRI, nonverbal, polymicrogyria, white matter connectivity

1 Introduction

The clinical phenotype of absent speech (HP:0001344, Human Phenotype Ontology, Köhler et al., 2021) lies at the most severe end of developmental alterations, signalling a complete failure of a key developmental outcome, rather than a developmental delay. The lack of speech development is a relatively frequent phenotype found across a myriad of neurodevelopmental disorders with sparse aetiologies and likely diverse underlying mechanisms. In particular, it frequently appears among the clinical sequelae of bilateral perisylvian polymicrogyria (BPP) (Braden et al. 2019), a brain malformation disturbing the laminar and gyral structure of the cortex around the sylvian fissure (Stutterd and Leventer 2014). The involvement of the perisylvian region, a primary seed of auditory language and motor functions, along with the frequent severe speech disruption, mark BPP as a valuable inroad into the neural mechanisms of speech and language. In this case report, we present a patient with BPP and no speech (age 12;4 years) and conduct a multimodal analysis to examine different aspects of auditory-speech circuity from early auditory processing to cortical integration with motor functions.

Absent speech in BPP is characterized as anarthria (Braden et al., 2019), a complete loss of neuromuscular control of speech production. Indeed, oro-motor dysfunction is core to the disorder (Jansen et al. 2005; Braden et al. 2021), manifesting in difficulties in tongue movement and swallowing, excessive drooling and disrupted speech. Cortical anarthria is caused by lesions to the frontal operculum

with minimal auditory and language problems (Kaga et al. 2004; Lucchelli and Papagno 2005). In children with cerebral palsy, it coexists with severe fine and gross motor deficits that restrict the ability to gesture or manipulate objects and with a severely compromised receptive language (Molinaro et al. 2020). BPP goes beyond the sole diagnosis of anarthria showing compromised expressive and receptive language (Braden et al. 2019) and disruptions in central auditory processing (Boscariol et al. 2010; Boscariol et al. 2011). A more severe language impairment in BPP, yet not necessarily absent speech as such, has been linked to two particular aspects of brain anatomy. One is a specific structural anomaly in a tract subserving the mapping of auditory speech to motor output, the arcuate fasciculus (AF), which has been shown to be non-detectable via diffusion MRI (dMRI) (Saporta et al. 2011; Kilinc et al. 2015; Paldino et al. 2015; Paldino et al. 2016; Oh et al. 2018). The other is a diffuse structural pattern with polymicrogyria extending along the entire sylvian fissure as opposed to the posterior parietal region (Braden et al., 2019). These findings highlight the complexity of the BPP phenotype and the need for a more comprehensive exploration of the regions along the sylvian fissure key to auditory-language processing to gain insights into the nature of speech and language impairment in BPP. This was the aim of this study in a case at the extreme end of speech impairment.

The structural malformation proper to polymicrogyria does not seem to trigger functional reorganization of the somatosensory or motor cortices (Burneo et al., 2014; Burneo et al., 2004; Nikolova et al., 2015). The neurons within the polymicrogyric cortex may and often do retain their sensibility to gross-motor stimulation under fMRI and TMS (Araujo et al., 2006; Burneo et al., 2014; Dumoulin et al., 2007; Innocenti et al., 2001; Janszky et al., 2003; Lenge et al., 2018; Munakata et al., 2006; Staudt et al., 2004). The underlying mechanisms for this retained function remain unclear. However, studies have linked two factors to decreased stimulus-sensitivity in the motor cortex: cortical thickening and local gyrification alteration (Lenge et al., 2018), and the integrity of motor white matter projection fibers (Munakata et al., 2006). While the functionality of language cortex has been minimally explored in BPP, studies reported activation to speech in the inferior frontal gyrus (IFG), but not the temporal regions (Araujo et al., 2006; Janszky et al., 2003). Thus, an extensive assessment of the auditory cortex is warranted specifically in terms of the two aforementioned factors linked to functionality: the degree of cortical thickening of the auditory cortex and the integrity of its thalamo-cortical projection fibres, the acoustic radiation (AR). It further raises questions about the intrinsic functional organization of the auditory cortex, thought to constitute a template for processing of upcoming stimuli (Teissier and Pierani 2021), a question currently unexplored in BPP. Conducting a comprehensive examination of these factors would complement the supposed marker of disordered language in BPP, specifically, the integrity of the AF discussed above.

While previous research using animal models of BPP has shown reductions or alterations of fibre tracts (Rosen et al. 2000), the specificity and biological significance of the AF non-detectability by dMRI needs further scrutiny. Beyond the AF agenesis, a considerable decrease in fibre coherence within the tract could also potentially lead to its non-detectability (Paldino et al., 2016). The limited

sensitivity of the traditional tractography approaches to fiber reconstruction, such as tensor-based deterministic tractography used in the studies on the AF in BPP (Kilinc et al., 2015; Oh et al., 2018; Paldino et al., 2016; Paldino et al., 2015; Saporta et al., 2011) hampers insights into this question. Here we have implemented probabilistic tractography based on constrained spherical deconvolution (CSD), which has shown higher sensitivity in resolving crossing fibres even in data of clinical quality, i.e., lower b-value (Tallus et al., 2023). Further challenging the specificity of the AF integrity as a marker of disordered language in BPP is a manual bundle segmentation implemented in the studies above, which may be challenging in patients with compromised anatomy. In this study, we employed an automated machine-learning-based segmentation, which has shown superior outcomes in patients with altered anatomy (Richards et al. 2021; Tallus et al. 2023), utilizing two fibre definitions. Along with the AF, we have also targeted the frontal aslant tract (FAT), a bundle connecting the IFG to the supplementary motor complex, whose integrity has been related to orofacial movement control in Foix-Chavany-Marie syndrome (Martino et al. 2012).

This study aims to provide a comprehensive and integrated analysis of various factors likely contributing to the absent speech phenotype in individuals with BPP. Specifically, it examines, in a case subject: (a) the degree of morphological disruption of the polymicrogyric cortex, assessing cortical thickness similar to Lenge et al (2018), relative to an on-site age-matched control and an archival control cohort from a publicly available dataset. In relation to the pattern of cortical disruption, we then explore (b) its sensitivity to speech stimuli, (c) its intrinsic functional organization (targeting the intrinsic auditory network reconstructed through independent component analysis), (d) the integrity of the auditory projection tract, and (e) the integrity of tracts subserving motor speech production, the AF and the FAT. We apply multifibre probabilistic tracking with two different tract segmentation approaches.

2 Material and methods

2.1 Transparency statement

We report how we determined our sample size, all data exclusions, all inclusion/exclusion criteria, whether inclusion/exclusion criteria were established prior to data analysis, all manipulations, and all measures in the study. No part of the study procedures or analyses was pre-registered prior to the research being conducted. This study was approved by an institutional review board (CEIm Hospital Ruber Internacional; Sa-15842/19-EC:385), in accordance with 1964 Helsinki declaration and its later amendments. All participants provided their informed consent to participate in the study. The conditions of our ethics approval do not permit public archiving of anonymized raw brain imaging or behavioural data. Readers seeking access to the data should contact the lead author Wolfram Hinzen (hinzen.wolfram@upf.edu). Access will be granted to named individuals in accordance with ethical procedures governing the reuse of sensitive data. Specifically, requestors must sign a collaboration

agreement. Legal copyright restrictions prevent public archiving of standardized assessment used in this study (specified in Table 2) which can be obtained from the copyright holders in the cited references.

2.1 Sample

A case subject with BPP was selected based on the clinical presentation of absent speech phenotype and a previous diagnosis of perisylvian polymicrogyria and was recruited from a special school devoted to developmental disorders severely affecting language. As a basis of comparison of some analysis methods (see below), an on-site healthy control matched to the case subject on age, handedness, and sex was also recruited. The on-site control was born at term with no complications and no personal or family history of language delay or neurodevelopmental disorders (verified through adapted *TPBA2* Child and Family History Questionnaire; Linder 2008). Further 25 healthy controls from an online open dataset (ABIDE-II, http://fcon_1000.projects.nitrc.org/indi/abide/abide_II.html) were also included. Sample demographics and data quality metrics are summarized in Table 1.

Table 1: Demographics and data quality metrics of the case subject and the control cohorts

		BPP patient	On-site control	Archival controls
Demographics	Age (years;months)	12;4	12;4	M = 13.1, SD = 1.3
	Sex	M	M	M
	Handedness	R	R	R
T1w	CNR	1.76	0.87	M = 1.51, SD = 0.18
	surface rating	5	5	M = 4.4, SD = 0.49
DWI	% outliers	1.2	1.6	
	CNR	17.4	1.34	
	RMSD (mm)	0.39	0.79	
	SNR	30.2	30.69	
EPI rest	SNR	2.14		
	FD %	76.52		
	gcor	0.025		
	tSNR	19.91		
EPI task	SNR	4.15		
	FD %	61.73		
	gcor	0.019		
	tSNR	31.05		

Note. CNR = **contrast-to-noise ratio; FD % = instantaneous head motion computed as percent of framewise displacement; gcor = global correlation;** RMSD motion **= mean head motion computed as** root mean square of displacement; SNR = **signal-to-noise ratio; surface rating = manual** quality assessment ratings for the surface reconstructions (5 indicated no inaccuracies, 4 indicates very minor inaccuracies); tSNR = temporal **signal-to-noise ratio.**

2.2 Case description

The patient was diagnosed with extensive perisylvian polymicrogyria at the age of 6 months after presenting with epileptic seizures, later controlled by medications (Oxcarbazepine). The first-year

developmental milestones were acquired with a delay, with social smile acquired at 3 months, head control at 8 months, rolling over at 15 months and walking at three years of age. Between two and three years of age, the patient was presenting with apparent normal prelinguistic and interactional behaviour, yet no production of articulated speech beyond guttural sounds, a profile that remains unchanged at the time of the study. The Merrill-Palmer developmental battery, administered at 3;4 years of age using alternative and augmentative communication system (AAC), yielded a global development at the level of 22 months, fine motor development at 19 months, receptive language at 27 months, memory at 29 months, cognition at 21 months and visuo-motor coordination reaching an 18-month age-equivalent. The patient started learning to write at 6 years of age distinguishing grammatical tense, number, and gender, complementing the preferred use of gestures and the communication device (LetMeTalk: Free AAC Talker) where he was constructing picture-based sentences of the type SVO. Genetic screening conducted via NGS for alterations related to disorders of neuronal migrations (including SRPX2), intellectual disability, and frequent genetic disorders revealed no genetic anomaly. Reduced or halted movement of orofacial musculature, including the tongue and the lips, were observed in an orofacial myofunctional assessment. External clinical examination of the pharynx showed no alterations.

At the time of the study (± 6 months), when the participant was 12 years old, several auditory and language assessments were performed. The examination of the external auditory canal via otoscopy was within the norm as was the hearing sensitivity to pure tones examined via audiometry. An auditory discrimination test of minimal pairs showed difficulties in distinguishing phonemes with a different place of articulation (see Supplementary information). Results of written and spoken language comprehension and nonverbal IQ assessments are shown in Table 2. Participant's speech production consisted of nonarticulated guttural sounds only, which he employed communicatively to demand and draw attention. Additionally, the participant exhibited a full range of early communicative gestures, as verified through parental reports using the MacArthur-Bates Communicative Development Inventories (Fenson et al. 2007). During the study period, the participant also utilized a text-to-speech application, specifically the Speech Assistant AAC. A sample of participant's spontaneous speech using Speech Assistant elicited through question prompts with and without visual aids can be found in Supplementary information. Similarly, an example of participant's word writing skills as assessed in school dictation can also be found in the Supplementary files.

Table 2: Language and nonverbal IQ assessments

Standartized test	Measure	Evaluation
PPVT-III	Verbal mental age	7;2 age-equivalent (RS = 82)
Nepsy-II	Comprehension of verbal instructions	low (RS = 4)
	Phonological processing	very low (RS = 2)
Prolec-R	Comprehension of written sentences	severe difficulty (RS = 13)
	Grammatical structures	severe difficulty (RS = 7)
	Oral comprehension	difficulty (RS = 2)
	Comprehension of textual narratives	difficulty (RS = 6)

Standartized test	Measure	Evaluation
CEG	Comprehension of grammatical structures	<1 percentil (RS = 49)
Matrices	General IQ	medium-low (IQ = 90, RS = 25)

Note. PPVT-III = Peabody Picture Vocabulary Test-III (Dunn & Dunn, 1997; Dunn et al., 2010); Nepsy-II = A Developmental Neuropsychological Assessment (Korkman et al. 2007); Prolec-R = Evaluation of processes of reading (Cuetos et al. 2012); CEG = Comprehension of grammatical structures – test battery (Mendoza et al. 2005); RS = raw score; Matrices (Sánchez-Sánchez et al. 2015) = A general intelligence test battery. A level C was administered corresponding to the age group of the test between 9 and 12 years.

2.3 MRI acquisition parameters (BPP patient and on-site control)

MRI data were collected at the Ruber International Hospital, Madrid, on a Siemens Prisma 3T scanner using a 64-channel head coil. The acquisition of a high-resolution T1-weighted (T1w) structural image (magnetization-prepared rapid-acquisition, gradient echo sequence; TR = 2,400 msec, TE = 2.22 msec, slice thickness = .7999 mm, 0.8 mm in plane resolution, 208 sagittal slices, matrix size = 300 x 320) was followed by a T2-weighted (T2w) structural image (TR = 3,200 msec, TE= 563 msec, slice thickness = .7999 mm, 208 sagittal slices, matrix size = 300 x 320). T1-weighted image of the BPP case subject is shown in Figure 1. Diffusion MRI data consisted of 64 slices (FOV = 230x230 mm, voxel size = 1.98 x 1.98 mm^2, TR = 4,600 msec, TE = 101 ms , flip angle = 90º, slice-thickness = 2 mm; acceleration factor = 2; b-value = 1250 s/mm^2; 30 diffusion gradient directions; 4 b0s, 1 with reversed phase encoding to correct for spatial distortions). After structural data was collected, resting state fMRI (no stimuli were presented during acquisition) was acquired. One functional run (8 min 52 sec) consisting of 264 functional images sensitive to blood oxygenation level-dependent contrast (BOLD; echo planar imaging (EPI) T2*-weighted gradient echo sequence; TR = 2,000 msec, TE = 30 msec, flip angle 80º, acquisition matrix = 576 x 576, 4.37 mm in plane resolution, 3.5 mm thickness, no gap, 32 axial slices aligned to the plane intersecting the anterior and posterior commissures) was acquired. Lastly, an fMRI acquisition with passive language stimulation was carried out (see below for details). One run (11 min 39 sec) was acquired consisting of 358 functional images (EPI T2*-weighted gradient echo sequence; TR = 2,000 msec, TE = 30 msec, flip angle 90º, acquisition matrix = 612 x 612, 2,35 mm in plane resolution, 3.5 mm thickness, no gap, 32 axial slices aligned to the plane intersecting the anterior and posterior commissures).

Figure 1: T1-weighted structural image of the BPP patient in sagittal, coronal, and axial planes.

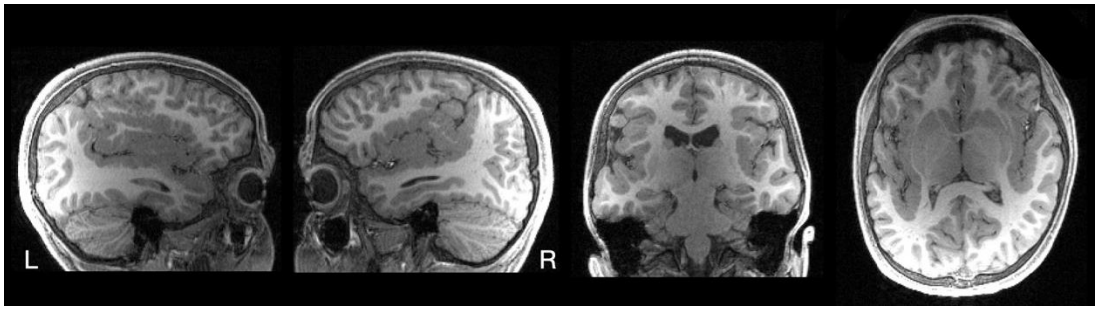

2.4 fMRI experimental design

Speech stimuli consisted of a spontaneous narration of a short children story (*The snowman* by Raymond Briggs) recorded in child-directed speech by a female native Spanish speaker. The story was divided in 10 blocks. Each block contained short sentences forming a sequence of complete phrases. An additional 10 blocks followed with the original story played backwards. The average block length was 20 sec (range = 18.7 – 21.76 sec). The stimuli blocks were presented in order (first those with the original story followed by blocks of reversed speech), with 15 sec rest periods between blocks where no stimuli were presented. The off-resting periods were set to 15 sec because the BOLD response in children returns to baseline levels faster than in adults (Richter and Richter 2003; Blasi et al. 2011).

2.5 MRI preprocessing

2.5.1 Structural MRI

Cortical reconstruction was performed with FreeSurfer version 5.3.0. The technical details of this procedure are described in prior publications (Dale et al. 1999; Fischl et al. 1999). Briefly, this processing includes removal of non-brain tissue using a hybrid watershed/surface deformation procedure (Ségonne et al. 2004), automated Talairach transformation, intensity normalization (Sled et al. 1998), tessellation of the gray matter white matter boundary, automated topology correction (Fischl et al. 2001; Ségonne et al. 2007), and surface deformation following intensity gradients to optimally place the gray/white and gray/cerebrospinal fluid borders at the location where the greatest shift in intensity defines the transition to the other tissue class. Cortical thickness was calculated as the closest distance from the gray/white boundary to the gray/CSF boundary at each vertex on the tessellated surface (Fischl and Dale 2000).

2.5.2 Functional MRI

EPI images were pre-processed with FMRIB's Software Libraries (FSL v5.0.10; Smith et al. 2004) and SPM12 (Wellcome Trust Centre for Neuroimaging, University College London, UK). A common preprocessing pipeline via fMRIPrep (version 1.5.0.) did not yield satisfactory results, with distorted brain mask detection and tissue segmentation that included non-cerebral tissue. Instead, an SPM12 standard pre-processing pipeline was implemented and included motion correction via rigid-body realignment, normalization to a 3 mm-isotropic MNI152 template, spatial-smoothing with a Gaussian kernel of 6 mm at full-width half maximum. Structural T1-weighted images were segmented using the default tissue probability maps. EPI images were corregistered to the structural images. Visual inspection of the pre-processed images was performed to assure quality.

Independent component analysis (ICA) was applied to resting state data using MELODIC (Multivariate Exploratory Linear Decomposition into Independent Components) Version 3.15, part of

FSL. The signal was filtered with high-pass Butterworth filter (0.008 Hz < f). An automatic dimensionality estimation was applied, and the resulting independent components (ICs) were inspected at individual and group level. Data were inspected for a component with a bilateral spatial distribution at the sylvian fissure and its time course was visually inspected.

For functional activation analysis, a block design matrix was specified in SPM12 using the canonical hemodynamic response function with one condition, 'Speech', which included both FWD and BWD stimuli blocs, given a lack of a differential response between FWD and BWD conditions (results not reported). Data were high pass filtered (to a maximum of 1/128 Hz). Previously estimated 6 movement parameters were included in the model as part of the nuisance regression. An explicit masking was applied using segmented grey matter images to restrict the analysis to the cortex and reduce the number of comparisons to increase power. 'Speech' contrast was estimated.

2.5.3 Diffusion MRI

The diffusion MRI data were preprocessed using an MRtrix3-based (version 3.0.3) workflow and included denoising, Gibbs Ringing Artifact removal, and eddy current correction (FSL's eddy toolbox). B1 field inhomogeneity correction was performed with ANTs (version 2.3.1). A fractional anisotropy (FA) map was used to estimate the rigid transformation to MNI space via FSL-FLIRT tool (version 6.0). Fibre orientation distributions (FODs) were estimated using single-shell multitissue-CSD algorithm for response functions of WM and CSF, part of MRtrix3.

2.6 Analyses

2.6.1 Cortical thickness outlier analysis

To estimate the degree of morphological differences of the patient's cortex, vertex-wise z-scores were calculated for the patient's CT map based on the mean and standard deviations within the healthy control group including the on-site and archival controls (Marquand et al. 2016). This Z-map was subsequently smoothed at FWHM 10 mm. A $|z| \geq 2$ threshold was applied to identify "outlier" clusters within the patient's CT map, with positive clusters indicating regions of abnormally greater cortical thickness and negative outlier clusters indicating abnormally lower cortical thickness compared to the control group. The surface area, location in the Desikan atlas (Desikan et al. 2006) and z-values of the cluster peaks are reported. The patient's CT map was transferred from fsaverage to patient's native surface using FreeSurfer's surf2surf tool and projected on the native inflated surface.

2.6.2 Intrinsic resting state and task-based functional analyses

The patient's task-derived activation map was smoothed at FWHM 6 mm, thresholded $p < .001$ uncorrected and projected onto the patient's T1-weighted image in MNI space. The location in the

Harvard-Oxford cortical and subcortical atlas and T-value at peak of the resulting clusters was reported. Similarly, the Z-map of an identified resting state bilateral component was smoothed at FWHM 6 mm, thresholded at $|z| \geq 3$, and projected onto the patient's T1-weighted image in MNI space. The location in the Harvard-Oxford cortical atlas and Z-value at peak of the resulting clusters was reported.

The statistical maps were moved to the fsaverage surface space using a registration fusion approach as implemented by brainSurfer (Teghipco 2022) and documented in Wu et al. (2018). The resting state map was binarized and projected onto fsaverage space along with the CT map for visual assessment of their spatial overlap. The unthresholded activation map was also visualized, projected onto the fsaverage space.

2.6.3 White matter tract segmentations and analyses

Bundle-specific segmentations were generated using TractSeg (Wasserthal et al. 2018), an automatic machine learning algorithm (https://github.com/MIC-DKFZ/TractSeg) trained on 72 major WM bundles as well as on bundles definitions as provided by XTRACT (Warrington et al., 2020). The AF was reconstructed following both the former (TractSeg-internal) and latter (XTRACT) bundle definitions, while the FAT and the AR were reconstructed based on the XTRACT bundle definitions only. Volume of the tracts was calculated as number of voxels occupied by the tract mask multiplied by voxel volume (1.25 mm^3). FA, mean diffusivity, radial diffusivity, and axial diffusivity were estimated and averaged over the tract masks. The bundle segmentations and metrics were compared to the on-site healthy control.

3 Results

3.1 Cortical thickness outlier analysis

Outlier analysis highlighted several regions of the cortex with abnormally greater cortical thickness (Figure 2) spanning frontal, temporal, and parietal cortices (Table 3).

Figure 2: BPP patient's Z-Map of increased cortical thickness

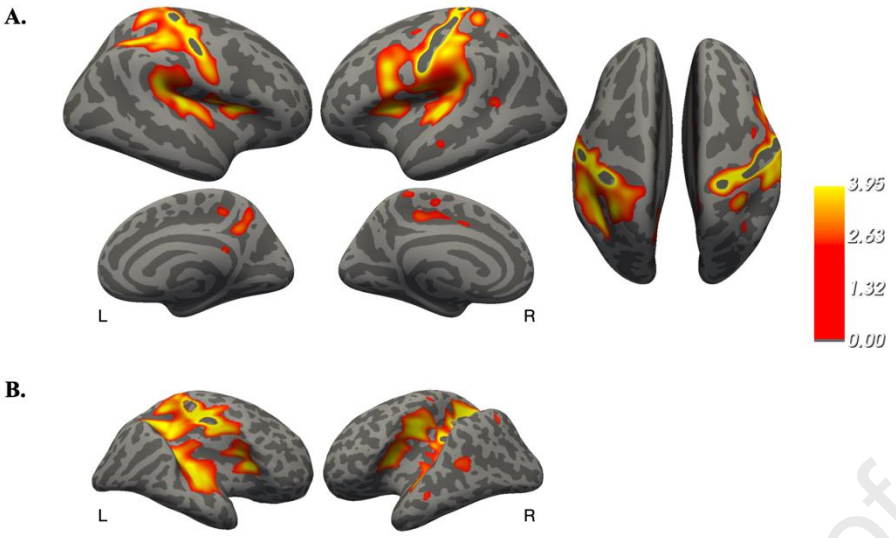

Note. A. shows the CT Z-map projected onto fsaverage surface. In B., the Z-map is projected onto the patients' native surface.

Table 3. Regions of abnormally increased cortical thickness

Region at cluster peak	Hemisphere	Z at peak	X	Y	Z	Area[mm^2]	NVtxs
postcentral	L	5.0	-37.8	-25.4	49.8	5023.87	12355
	R	3.8	26.0	-32.7	51.3	315.83	874
transversetemporal	L	4.5	-35.6	-28.5	13.0	2163.13	5178
superiortemporal	R	2.3	46.4	-17.6	-10.3	33.27	82
parsopercularis	L	4.5	-33.6	10.8	11.9	739.35	2084
bankssts	R	2.5	44.7	-40.9	13.1	120.51	356
precentral	R	5.0	32.4	-17.7	43.1	7362.70	17887
		2.3	40.2	-3.7	43.4	59.50	120
paracentral	R	2.8	17.8	-29.2	38.0	253.39	751
		2.5	10.0	-35.1	61.6	76.28	223
		2.3	6.9	-17.1	51.2	83.68	159
superiorparietal	R	2.3	28.0	-47.5	42.1	84.86	225
precuneus	L	3.2	-14.2	-47.9	35.1	427.99	896
		2.8	-18.0	-38.7	45.2	82.28	242
isthmuscingulate	L	2.5	-7.2	-39.7	22.9	28.80	95

Note. Z at peak = the maximum *z-value* in cluster; XYZ = the Talairach (MNI305) coordinate of the maximum; Area = surface area (mm^2) of cluster; NVtxs = number of vertices in cluster.

3.2 Intrinsic resting state and task-based functional analyses

Independent component analysis identified a single bilateral perisylvian resting state network (Figure 3) centred at the central opercular cortex, and the post- and precentral gyrus (Table 4), partially extending into the Heschl's gyrus (in white contour).

Figure 3. BPP patient's bilateral perisylvian resting state network

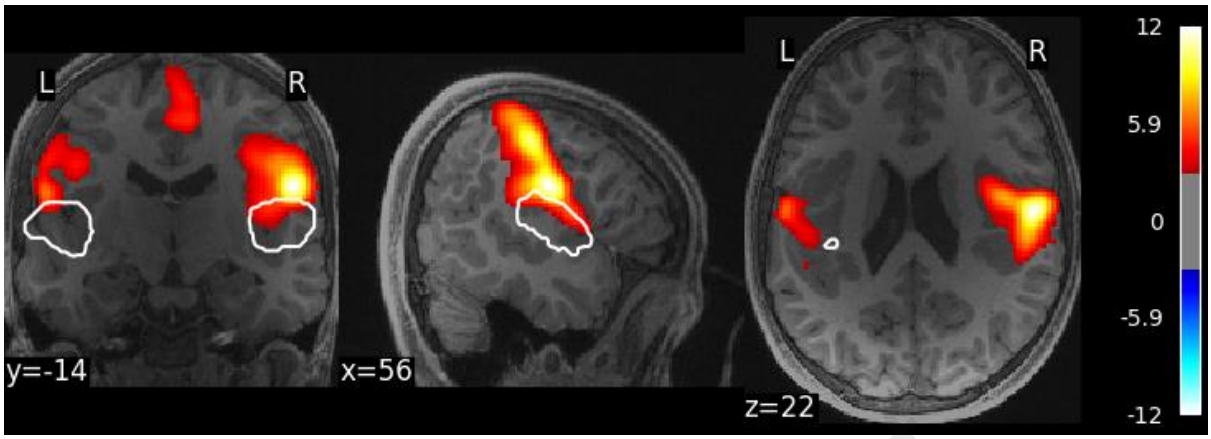

Note. The Z-map is overlaid on the BPP patient's T1-weighted image in MNI152 space. In white, the contours of the Heschl's gyrus are represented according to the Harvard-Oxford Cortical and Subcortical atlas.

Table 4: Regions of the bilateral perisylvian resting state network

Region at cluster peak	Hemisphere	Z at peak	X	Y	Z	Size(vox)
central opercular cortex	R	11.8	56	-14	22	6353
postcentral gyrus	L	6.44	-58	-12	18	1942
precentral gyrus	R	6.01	4	-20	66	1046
undefined*		3.32	-32	-34	-34	18
temporal occipital fusiform cortex	L	3.33	-32	-54	-22	11

Note. Regions given according to the Harvard-Oxford Cortical and Subcortical Structural Atlas; Z at peak = the maximum *z-value* in cluster; XYZ = MNI coordinates of the peak; Size = cluster extent in voxels. * Region undefined in Harvard-Oxford Cortical and Subcortical Structural Atlas. However, in Neurosynth, area within 2 mm of the coordinates was identified with Cerebellum.

Figure 4: The overlap of the BPP patient's bilateral perisylvian resting state network with the map of increased cortical thickness

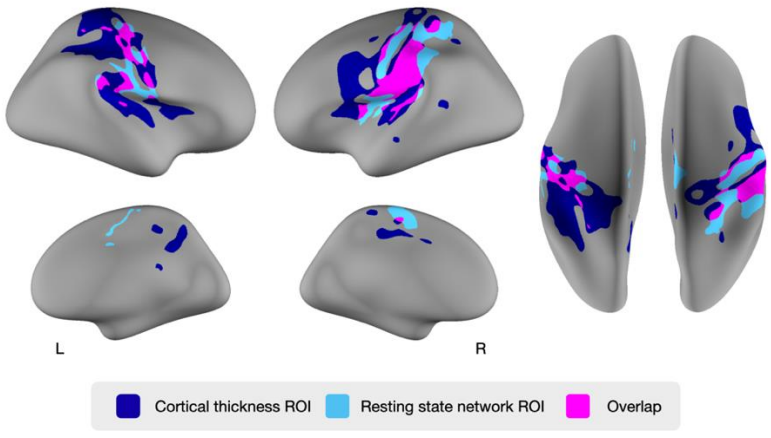

Note. The resting state network and the CT map are projected onto the fsaverage surface.

Auditory speech stimulation did not yield any significant suprathreshold cortical activations, but significant activations were observed subcortically in the bilateral thalamus and the right midbrain (Figure 5, Table 5). Subthreshold activations to Speech are shown in Supplementary material (Figure S1), projected on fsaverage surface space for visual reference to cortical thickness outlier analysis.

Figure 5. BPP patient's map of activation to Speech stimuli at p < .001 uncorrected

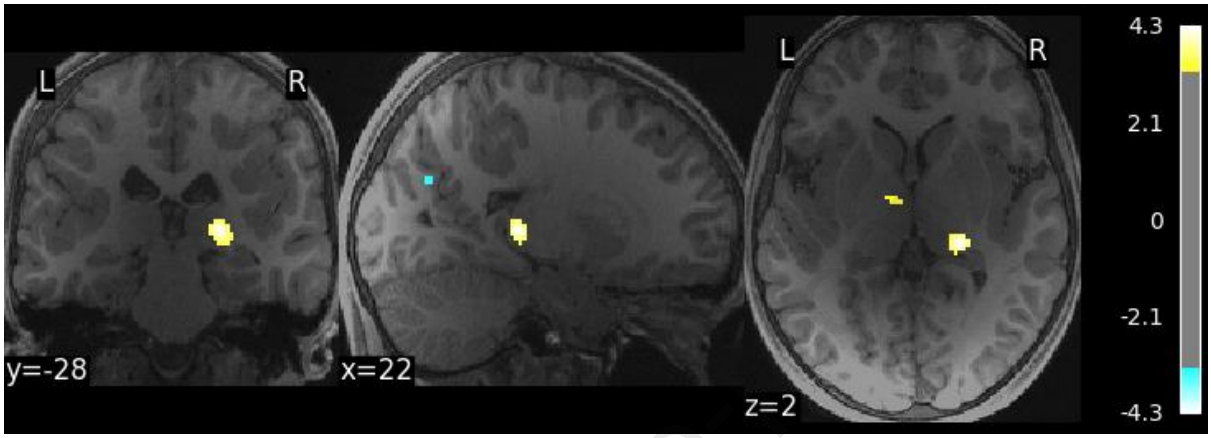

Note. The T-map is overlaid on the BPP patient's T1-weighted image in MNI152 space.

Table 5: Regions of suprathreshold activation to Speech stimuli with a cluster size > 10

Region at cluster peak	Hemisphere	T at peak	X	Y	Z	Size(vox)
thalamus	R	4.26	22	-28	2	27
	L	3.77	-8	-10	0	43
undefined*	R	3.43	8	-20	-12	26

Note. Regions given according to the Harvard-Oxford Cortical and Subcortical Structural Atlas; T at peak = the maximum T-value in cluster; XYZ = MNI coordinates of the peak; Size = cluster extent in voxels. * Region undefined in Harvard-Oxford Cortical and Subcortical Structural Atlas. In Neurosynth, the region was identified as right midbrain.

3.3 Bundle reconstructions of the AR, the FAT, and the AF based on Xtract and TractSeg templates

3.3.1 Xtract template

Figure 6 shows bundle segmentations of AR, the FAT and the AF in the BPP case and the on-site control. The AR of the BPP case could be traced from the thalamus bilaterally, but fully reaching the Heschl's gyrus only in the right hemisphere (volume = 988.8 mm^3 and 2 383.8 mm^3 of the left and right AR, respectively). His FAT could be traced from the superior frontal gyrus bilaterally, extending towards the inferior frontal gyrus, yet not reaching it in fully extent in the right hemisphere (volume = 2 905 mm^3 and 1 848.8 mm^3 of the left and right FAT, respectively). The arc of his AF was not fully reconstructed bilaterally, yet the ending segmentations in the frontal and temporal cortices could be

appreciated (volume = 1 893.8 mm^3 and 3 077.5 mm^3 of the left and right AF, respectively). All three tracts were fully reconstructed in the on-site control (left AR = 2 928.8 mm^3, right AR = 2 916.3 mm^3; left FAT = 5 481.3 mm^3, right FAT = 4 623.8 mm^3; left AF = 10 565 mm^3, right AF = 11 966.3 mm^3).

Figure 6. Xtract-based bundle segmentations of the AR, the FAT, and the AF

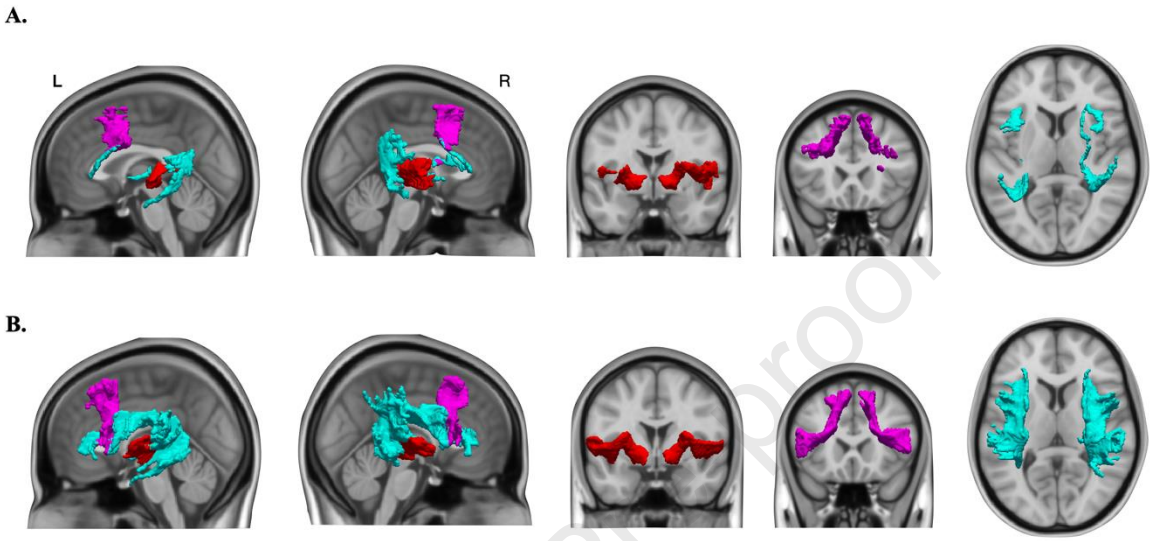

Note. The AR (in red), the FAT (in purple) and the AF (in cyan) in the BBP patient (A) and the on-site control (B). Bundles are overlayed on MNI152 T1-weighted template.

3.3.2 TractSeg template

TractSeg fully reconstructed both the left AF (volume = 41 333.8 mm^3, FA = 0.273, MD = 0.769e-03, RD = 0.654e-03, AD = 0.998e-03) and right AF (volume = 42 196.3 mm^3, FA = 0.286, MD = 0.762e-03, RD = 0.644e-03, AD = 0.999e-03) in the BPP patient including the arc of the AF (Figure 7). The left AF (volume = 61 505 mm^3, FA = 0.260, MD = 0.770e-03, RD = 0.662e-03, AD = 0.985e-03) and right AF (volume = 60 363.8 mm^3, FA= 0.265, MD = 0.777e-03, RD = 0.667e-03, AD = 0.997e-03) segmentations in the on-site controls are shown in Figure 7.

Figure 7: TractSeg-based bundle segmentation of the AF

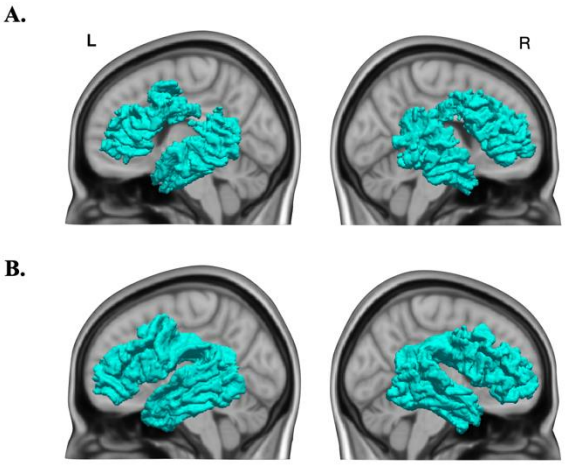

Note. The AF (in cyan) in the BBP patient (A) and the on-site control (B). Bundles are overlayed on MNI152 T1-weighted template.

4 Discussion

The absent speech phenotype spans sparse disorder aetiologies and underlying mechanisms. Absent speech in bilateral perisylvian polymicrogyria (BPP) has been linked to anarthria, a loss of neuromuscular control of speech production. Beyond this sole characterization, the malformation core to BPP alters the cortical structure of the extensive perisylvian cortex and presumably the underlying white matter circuity. In this study, we explored two aspects of brain anatomy associated with BPP and severe language impairment in a case at the extreme of this severity (i.e., absent speech), namely the spatial extent of the polymicrogyric cortex and the detectability of the arcuate fasciculus, crucially involved in speech production. We then moved to explore, for the first time, the degree of structural and functional alteration of the perisylvian cortex, underlying auditory-speech processing, at the core of this malformation.

In line with the cognitive profile reported in BPP, the present BPP case with absent speech showed disrupted central auditory processing manifesting in altered phoneme discrimination with normotypical appearing external auditory canal and preserved sensitivity to pure tones. Both the visual examination by an expert radiologist and the cortical thickness outlier analysis yielded extensive regions of abnormality spanning the temporal lobe along with frontal and parietal regions. This is in line with previous observations of widespread polymicrogyria in cases with severe language impairment and underscores the complexity of the phenotype, which cannot be easily explained by single robust links to a specific disorder, genetic mutation, or anatomical structure.

Our results challenge the significance of the non-detectable AF as a potential biomarker of severe language impairment in BPP. The discrepancy between the bilateral reconstruction of the AF in the present study compared to past studies likely stems from methodological limitations of the traditional methods implemented in the previous reports. Our approach modelled several fibre

orientations increasing robustness to crossing fibres and implemented two automated bundle segmentations considering both the fibre shape and spatial relation to anatomical regions. While absence of the AF in an absolute sense is unlikely, the success of the present method could signal its robustness even to tissues with marked disorganization, flagged as the AF absence by the traditional tractography approaches (Saporta et al. 2011; Kilinc et al. 2015; Paldino et al. 2015; Oh et al. 2018). The volume of the fully segmented AF, achieved by a more broad and complete TractSeg bundle definition, was comparable to the healthy control, as was its microstructural integrity indexed by all four DWI metrics. Yet, when the bundle definition was more stringent and specific, like the Xtract one, the AF was not fully reconstructed specifically along the arching segment. Overall, our findings challenge the hypothesis that a disrupted AF is at the core of major speech production deficits in severe cases with polymicrogyria. To expand on possible involvement of anatomical structures linked to speech production, we examined the FAT previously related to orofacial movement control in Foix-Chavany-Marie syndrome (Martino et al. 2012). In our specific case, the FAT was reconstructed to a great extent showing FA-based microstructural integrity similar if not higher to that of a heathy control, likely due to the tract reconstruction including less perimeter regions with lower FA value. In conclusion, white matter alterations typically associated to speech and oromotor difficulties cannot fully account for the clinical profile of BPP.

A promising avenue to elucidate speech production deficits in BPP is a deeper anatomico-functional exploration of the auditory-language cortex, a core region of cortical alteration characteristic of BPP. Indeed, regions of maximal cortical thickening were observed in the left transverse temporal gyrus and pars opercularis, along with the precentral and postcentral gyri, which aligns with Lenge et at. (2018). Such profound anatomical disruption could have significant functional consequences akin to the limited sensitivity to stimuli observed in the thickened motor cortex (Lenge et al. 2018; Munataka et al. 2008). In our specific case of BPP, there was a notable absence of suprathreshold cortical activation in response to speech stimuli, even in the frontal lobes where activations were observed previously (Araujo et al 2003; Janszky et al. 2005). However, it is worth noting that subcortical structures, such as the bilateral thalamus and midbrain, which are implicated in early stages of auditory processing, exhibited heightened sensitivity to speech stimuli. It appears that while the cortical regions affected by polymicrogyria may exhibit impaired responsiveness, the early subcortical structures in BPP could potentially bear a greater functional burden, speaking to the altered central auditory processing reported here and elsewhere. However, unlike adult cases of central auditory deficits resulting from cortical or subcortical lesions that lead to unresponsiveness to any type of sound, the present BPP maintained responsiveness to sound and retained auditory comprehension, albeit with notable difficulties.

One potential factor that may contribute to the disrupted functionality of the polymicrogyric cortex might be an altered integrity of the projection fibres responsible for conveying information to the cortex. Previous research (Munataka et al. 2008) indeed suggests a relationship between the integrity

of the motor pathways and cortical functionality. Damage to the AR could also lead to cortical deafness and dysarthria (Narayanan et al. 2017). However, in contrast to these findings, the auditory projection pathway was relatively preserved in our specific case. The microstructural integrity of the AR, as measured by the FA, was comparable to that of a healthy control, albeit the AR was fully reconstructed only in the right hemisphere. The relative preservation of the anatomical structures necessary for cortical processing contrasts with the observed lack of functional sensitivity of the auditory cortex, suggesting that factors beyond the integrity of projection fibers may be implicated in the functionality of the polymicrogyric cortex.

On that account, an intrinsic functional assembly of the auditory cortex was also lacking in the present case. The intrinsic auditory network emerges in development even before the opening of the sensory channels (Vasung et al. 2019) and is hypothesized to constitute a template of the characteristic functional circuity for processing of upcoming inputs (Teissier and Pierani 2021). In line with this premise, abnormal laminar and gyral structure of the cortex could impair the intrinsic functional organization and later processing of stimuli. Yet, motor regions did exhibit an intrinsic functional network. This observation carries two important implications. Firstly, it raises questions regarding the absence of intrinsic functional coupling in auditory regions, considering that clinical paediatric MRI susceptibility to movement artifacts would not explain why motor regions exhibit such coupling while auditory regions do not. Secondly, the functional severing of regions specifically associated with auditory processing raises questions regarding the impact of the degree of cortical alteration on functionality. It is indeed intriguing why regions associated with motor processing, which also exhibit significant cortical thickness abnormalities, do not appear to be as functionally severed as regions involved in auditory processing. In fact, the spatial pattern of this intrinsic network shows a considerable overlap with regions of cortical thickening. Understanding the interplay between cortical and subcortical structures in BPP appears crucial for elucidating the mechanisms of altered functionality.

Conclusions

This study has brought forth several unanswered questions regarding the functional and structural organization of the polymicrogyric cortex and its implications for the behavioural phenotype of BPP. It is intriguing to note that while the structural integrity of the auditory projection pathway, the AR, appears to be largely preserved in BPP despite severe cortical thickening, the intrinsic functional organization of the auditory cortex does not seem to be established and lacks sensitivity to external stimuli. Instead, the subcortical structures may assume a significant role in auditory processing. Interestingly, in contrast to the auditory cortex, the intrinsic functional organization of the motor cortex remained intact, as did both the AF and the FAT to a large extent, which are arguably involved in transmitting the articulatory code for motor cortex execution. This raises the question of alternative

neural markers underlying absent speech in BPP, which should be considered alongside the functional dysregulation of the auditory cortex.

This case study serves as an illustration of the limitations and the open questions of previously proposed markers of language in BPP and emphasizes the importance of using comprehensive methods when studying the absent speech phenotype. Future studies should focus on investigating the impact of cortical alteration in BPP and its interaction with the subcortico-cortical auditory circuitry. This case study also raises implications for studies aiming to establish robust links between singular MRI modalities or brain structures and altered speech and language development.

Data and code availability

The data at summary level (the patient's functional and CT statistical maps and bundle segmentations) as well as the analysis and figure plotting code are available at: https://osf.io/yxjsf/

Declaration of Competing Interest

The authors declare that they have no known competing financial interests or personal relationships that could have appeared to influence the work reported in this paper.

Acknowledgements

This work was supported by the Querer Foundation, Generalitat de Catalunya (AGAUR) and European Social Found (2018FI_B_00860 to D.S. and 2017-SGR-1265 to W.H.) and Ministerio de Economía y Competitividad (FFI2013-40526P and PID2019-105241GB-I00 to W.H.). Authors would like to thank Julia Elena Pardo for designing protocol and collecting spontaneous speech samples.

References

Araujo D, Araujo DB De, Pontes-neto OM, Escorsi-rosset S, Simao GN, Wichert-ana L, Velasco TR, Sakamoto AC, Leite JP, Santos AC. 2006. Language and Motor f MRI Activation in Polymicrogyric Cortex. 47(3):589–592.

Blasi A, Mercure E, Lloyd-Fox S, Thomson A, Brammer M, Sauter D, Deeley Q, Barker GJ, Renvall V, Deoni S, et al. 2011. Early specialization for voice and emotion processing in the infant brain. Curr Biol [Internet]. 21(14):1220–1224. https://doi.org/10.1016/j.cub.2011.06.009

Boscariol M, Abraa C, Garcia VL, Mantovani M. 2011. Auditory processing disorder in patients with language-learning impairment and correlation with malformation of cortical development. 33:824–831. https://doi.org/10.1016/j.braindev.2010.12.006

Boscariol M, Garcia VL, Guimarães CA, Montenegro MA, Hage SRV, Cendes F, Guerreiro MM.

2010. Auditory processing disorder in perisylvian syndrome. Brain Dev. 32(4):299–304. https://doi.org/10.1016/j.braindev.2009.04.002

Braden RO, Boyce JO, Stutterd CA, Pope K, Goel H, Leventer RJ, Scheffer IE, Morgan AT. 2021. Speech, Language, and Oromotor Skills in Patients With Polymicrogyria. Neurology. 96(14).

Braden RO, Leventer RJ, Jansen A, Scheffer IE, Morgan AT. 2019. Speech and language in bilateral perisylvian polymicrogyria: a systematic review. Dev Med Child Neurol. 61(10):1145–1152. https://doi.org/10.1111/dmcn.14153

Burneo JG, Bartha R, Gati J, Parrent A, Steven DA. 2014. 4-T fMRI of the motor and sensory cortices in patients with polymicrogyria and epilepsy. Clin Neurol Neurosurg [Internet]. 122:29–33. https://doi.org/10.1016/j.clineuro.2014.03.020

Burneo JG, Kuzniecky RI, Bebin M, Knowlton RC. 2004. Cortical reorganization in malformations of cortical development. A magnetoencephalographic study. Neurology. 63(10).

Cuetos F, Rodríguez B, Ruano E, Arribas D. 2012. PROLEC-R. Batería de Evaluación de los Procesos Lectores - Revisada. Madrid: TEA Ediciones.

Dale AM, Fischl B, Sereno MI. 1999. Cortical surface-based analysis. I. Segmentation and surface reconstruction. Neuroimage. 9:179–194.

Desikan RS, Segonne F, Fischl B, Quinn BT, Dickerson BC, Blacker D, Buckner RL, Dale AM, Maguire RP, Hyman BT, et al. 2006. An automated labeling system for subdividing the human cerebral cortex on MRI scans into gyral based regions of interest. Neuroimage. 31:968–980.

Dumoulin SO, Jirsch JD, Bernasconi A. 2007. Functional organization of human visual cortex in occipital polymicrogyria. Hum Brain Mapp. 28(12):1302–1312. https://doi.org/10.1002/hbm.20370

Dunn Leota M., Dunn Lloyd M. 1997. Peabody picture vocabulary test-III. 3rd ed. Circle Pines, MN: American Guidance Service.

Dunn Lloyd M., Dunn Leota M., Arribas Águila D. 2010. PPVT-III. Peabody, Test de vocabulario en imágenes [Internet]. 2nd Edition. Madrid: TEA Ediciones; [accessed 2018 Jun 7]. https://libreriaites.com/2041-ppvt-iii-peabody-test-de-vocabulario-en-imágenes-manual.html

Fenson L, Marchman VA, Thal DJ, Dale PS, Reznick JS, Bates E. 2007. MacArthur-Bates communicative development inventories. 2nd ed. Baltimore: Paul H. Brookes.

Fischl B, Dale AM. 2000. Measuring the thickness of the human cerebral cortex from magnetic resonance images. Proc Natl Acad Sci. 97:11050–11055.

Fischl B, Liu A, Dale AM. 2001. Automated manifold surgery: Constructing geometrically accurate and topologically correct models of the human cerebral cortex. IEEE Trans Med Imaging. 20(1):70–80.

Fischl B, Sereno MI, Dale AM. 1999. Cortical surface-based analysis: II: inflation, flattening, and a surface-based coordinate system. Neuroimage. 9(2):195–207.

Innocenti GM, Maeder P, Knyazeva MG, Fornari E, Deonna T. 2001. Functional activation of microgyric visual cortex in a human. Ann Neurol. 50(5):672–676. https://doi.org/10.1002/ana.1228

Jansen AC, Leonard G, Bastos AC, Esposito-Festen JE, Tampieri D, Watkins K, Andermann F, Andermann E. 2005. Cognitive functioning in bilateral perisylvian polymicrogyria (BPP): Clinical and radiological correlations. Epilepsy Behav. 6(3):393–404. https://doi.org/10.1016/j.yebeh.2005.01.012

Janszky J, Ebner A, Kruse B, Mertens M, Jokeit H, Seitz RJ, Witte OW, Tuxhorn I, Woermann FG. 2003. Functional organization of the brain with malformations of cortical development. Ann Neurol. 53(6):759–767. https://doi.org/10.1002/ana.10545

Kaga K, Nakamura M, Takayama Y, Momose H. 2004. A case of cortical deafness and anarthria. Acta Otolaryngol. 124(2). https://doi.org/https://doi.org/10.1080/00016480310015975

Kilinc O, Ekinci G, Demirkol E, Agan K. 2015. Bilateral agenesis of arcuate fasciculus demonstrated by fiber tractography in congenital bilateral perisylvian syndrome. Brain Dev [Internet]. 37(3):352–355. https://doi.org/10.1016/j.braindev.2014.05.003

Köhler S, Gargano M, Matentzoglu N, Carmody LC, Lewis-Smith D, Vasilevsky NA, Danis D, Balagura G, Baynam G, Brower AM, et al. 2021. The human phenotype ontology in 2021. Nucleic Acids Res. 49(D1):D1207–D1217. https://doi.org/10.1093/nar/gkaa1043

Korkman M, Kirk U, Kemp S. 2007. NEPSY - Second Edition (NEPSY - II). [place unknown]: APA PsycTests. https://doi.org/https://doi.org/10.1037/t15125-000

Lenge M, Barba C, Montanaro D, Aghakhanyan G, Frijia F, Guerrini R. 2018. Relationships Between Morphologic and Functional Patterns in the Polymicrogyric Cortex. Cereb Cortex. 28(3):1–11. https://doi.org/10.1093/cercor/bhx036

Linder T. 2008. Child and family history questionnaire. In: Transdiscipl Play Assess. 2nd ed. [place unknown].

Lucchelli F, Papagno C. 2005. Is slowly progressive anarthria a “pure” motor-speech disorder? Evidence from writing performance. Behav Cogn Neurosci. 11.

Marquand AF, Rezek I, Buitelaar J, Beckmann CF. 2016. Understanding heterogeneity in clinical cohorts using normative models: Beyond case-control studies. Biol Psychiatry. 80(7):552–561.

Martino J, de Lucas EM, Ibáñez-Plágaro FJ, Valle-Folgueral JM, Vázquez-Barquero A. 2012. Foix-Chavany-Marie syndrome caused by a disconnection between the right pars opercularis of the inferior frontal gyrus and the supplementary motor area. J Neurosurg [Internet]. 117(5):844–850. https://doi.org/10.3171/2012.7.JNS12404

Mendoza E, Carballo G, Muñoz J, Fresneda MD. 2005. Test de comprensión de estructuras gramaticales (CEG). [place unknown]: TEA Ediciones.

Molinaro M, Broman AT, Rathouz PJ, Hustad KC. 2020. Longitudinal Development of Receptive Vocabulary in Children with Cerebral Palsy and Anarthria: Use of the MacArthur-Bates CDI. Dev Neurorehabil [Internet]. 23(5):285–293. https://doi.org/10.1080/17518423.2019.1646829

Munakata M, Onuma A, Takeo K, Oishi T, Haginoya K, Iinuma K. 2006. Morphofunctional organization in three patients with unilateral polymicrogyria: Combined use of diffusion tensor

imaging and functional magnetic resonance imaging. Brain Dev. 28(6):405–409. https://doi.org/10.1016/j.braindev.2005.12.003

Narayanan S, Majeed KA, Subramaniam G, Narayanan A, Navaf KM. 2017. A Case of Cortical Deafness due to Bilateral Heschl Gyrus Infarct. Case Rep Med. 2017:3–5. https://doi.org/10.1155/2017/6816748

Nikolova S, Bartha R, Parrent AG, Steven DA, Diosy D, Burneo JG. 2015. Functional MRI of neuronal activation in epilepsy patients with malformations of cortical development. Epilepsy Res [Internet]. 116:1–7. https://doi.org/10.1016/j.eplepsyres.2015.06.012

Oh Y-B, Lee HN, Kim G-W, Won YH, Ko M-H, Seo J-H, Park S-H. 2018. Absence of Arcuate Fasciculus in a Child with Bilateral Perisylvian Polymicrogyria. Brain & Neurorehabilitation. 11(2). https://doi.org/10.12786/bn.2018.11.e14

Paldino MJ, Hedges K, Gaab N, Galaburda AM, Grant PE. 2015. Failure to Identify the Left Arcuate Fasciculus at Diffusion Tractography is a Specific Marker of Language Dysfunction in Pediatric Patients with Polymicrogyria. Behav Neurol. 2015. https://doi.org/10.1155/2015/351391

Paldino MJ, Hedges K, Golriz F. 2016. The arcuate fasciculus and language development in a cohort of pediatric patients with malformations of cortical development. Am J Neuroradiol. 37(1):169–175. https://doi.org/10.3174/ajnr.A4461

Richards TJ, Anderson KL, Anderson JS. 2021. Fully Automated Segmentation of the Corticospinal Tract Using the TractSeg Algorithm in Patients with Brain Tumors. Clin Neurol Nuerosurgery [Internet]. in press. https://doi.org/10.1016/j.clineuro.2021.107001

Richter W, Richter M. 2003. The shape of the fMRI BOLD response in children and adults changes systematically with age. Neuroimage. 20(2):1122–1131. https://doi.org/10.1016/S1053-8119(03)00347-1

Rosen GD, Burstein D, Galaburda AM. 2000. Changes in Efferent and Afferent Cerebrocortical Microgyria. J Comp Neurol. 418:423–440.

Sánchez-Sánchez F, Santamaría P, Abad FJ. 2015. Matrices. Test de Inteligencia General.

Saporta ASD, Kumar A, Govindan RM, Sundaram SK, Chugani HT. 2011. Arcuate fasciculus and speech in congenital bilateral perisylvian syndrome. Pediatr Neurol [Internet]. 44(4):270–274. https://doi.org/10.1016/j.pediatrneurol.2010.11.006

Ségonne F, Dale AM, Busa E, Glessner M, Salat D, Hahn HK, Fischl B. 2004. A hybrid approach to the skull stripping problem in MRI. Neuroimage. 22(3):1060–1075. https://doi.org/https://doi.org/10.1016/j.neuroimage.2004.03.032

Ségonne F, Pacheco J, Fischl B. 2007. Geometrically Accurate Topology-Correction of Cortical Surfaces Using Nonseparating Loops. IEEE Trans Med Imaging. 26(4):518–529. https://doi.org/https://doi.org/10.1109/TMI.2006.887364

Sled JG, Zijdenbos AP, Evans A. 1998. A nonparametric method for automatic correction of intensity nonuniformity in MRI data. IEEE Trans Med Imaging. 17:87–97.

Smith SM, Jenkinson M, Woolrich MW, Beckmann CF, Behrens TEJ, Johansen-Berg H, Bannister PR, Luca M De, Drobnjak I, Flitney DE, et al. 2004. Advances in functional and structural MR image analysis and implementation as FSL. Neuroimage. 23:S208–S219.

Staudt M, Krägeloh-Mann I, Holthausen H, Gerloff C, Grodd W. 2004. Searching for motor functions in dysgenic cortex: a clinical transcranial magnetic stimulation and functional magnetic resonance imaging study. J Neurosurg. 101:69–77. https://doi.org/https://doi.org/10.3171/ped.2004.101.2.0069

Stutterd CA, Leventer RJ. 2014. Polymicrogyria: A common and heterogeneous malformation of cortical development. Am J Med Genet Part C Semin Med Genet. 166(2):227–239. https://doi.org/10.1002/ajmg.c.31399

Tallus J, Mohammadian M, Kurki T, Roine T, Posti JP, Tenovuo O. 2023. A comparison of diffusion tensor imaging tractography and constrained spherical deconvolution with automatic segmentation in traumatic brain injury. NeuroImage Clin [Internet]. 37(May 2022):103284. https://doi.org/10.1016/j.nicl.2022.103284

Teghipco A. 2022. brainSurfer. Zenodo [Internet]. https://zenodo.org/record/7271544

Teissier A, Pierani A. 2021. Wiring of higher-order cortical areas: Spatiotemporal development of cortical hierarchy. Semin Cell Dev Biol [Internet]. 118(xxxx):35–49. https://doi.org/10.1016/j.semcdb.2021.05.010

Vasung L, Abaci Turk E, Ferradal SL, Sutin J, Stout JN, Ahtam B, Lin PY, Grant PE. 2019. Exploring early human brain development with structural and physiological neuroimaging. Neuroimage [Internet]. 187(July 2018):226–254. https://doi.org/10.1016/j.neuroimage.2018.07.041

Wasserthal J, Neher P, Maier-Hein KH. 2018. TractSeg - Fast and accurate white matter tract segmentation. Neuroimage [Internet]. 183(March):239–253. https://doi.org/10.1016/j.neuroimage.2018.07.070

Wu J, Ngo GH, Greve D, Li J, He T, Fischl B, Eickhoff SB, Yeo BTT. 2018. Accurate nonlinear mapping between MNI volumetric and FreeSurfer surface coordinate systems. Hum Brain Mapp. 39(9):3793–3808. https://doi.org/10.1002/hbm.24213

RediT author statement

Dominika Slušná: Conceptualization, Methodology, Software, Formal analysis, Investigation, Writing – Original draft preparation, Visualization. **Jiwandeep Singh Kohli:** Software, Formal analysis, Writing - Original draft preparation, Writing- Reviewing and Editing. **Janice Hau:** Validation, Investigation, Writing - Reviewing and Editing. **Juan Álvarez-Linera Prado:** Resources. **Annika Carola Linke:** Validation, Writing - Reviewing and Editing. **Wolfram Hinzen:** Writing- Reviewing and Editing, Supervision, Funding acquisition.